Optical Materials 116 (2021) 111100

Contents lists available at ScienceDirect

Optical Materials

journal homepage: http://www.elsevier.com/locate/optmat

Research Article

Sustainable carbon-based nanostructures with optoelectronic performance inspired by crustacean shells towards biomimetic pyrolysis and hydrothermal liquid crystal transfer

Trang The Lieu Chau [a,**], Tuyen Phi Vu [b,***], Hoa Thi Le [a], Do Van Phan [c], Ca Xuan Nguyen [d], Thanh Duy Luong [c], Phuong Thi Anh Le [e], Nhan Thi Thanh Dang [f], Long Viet Nguyen [g], Nguyen Duc Cuong [a,h,*]

[a] Department of Chemistry, University of Sciences, Hue University, 77 Nguyen Hue, Hue, 530000, Viet Nam
[b] Center for High Technology Development, 18 Hoang Quoc Viet, Hanoi, 100000, Viet Nam
[c] Thuyloi University, 175 Tayson, Hanoi, 100000, Viet Nam
[d] Faculty of Physics and Technology, Thai Nguyen University of Science, Thai Nguyen, 250000, Viet Nam
[e] Ba Ria Vung Tau University, 80 Truong Cong Dinh Street, Vung Tau, 790000, Viet Nam
[f] Department of Chemistry, Hue University of Education, Hue University, 34 Le Loi, Hue, 530000, Viet Nam
[g] Saigon University, An Duong Vuong, Ho Chi Minh, 700000, Viet Nam
[h] School of Hospitality and Tourism, Hue University, 22 Lam Hoang, Vy Da Ward, Hue, 530000, Viet Nam

ARTICLE INFO

Keywords:
Rod-shaped chitin liquid crystals
Biomimetic carbonization
Hierarchical pores
Hydrothermal liquid crystal phase transfer
Photoluminescent hydrophobic carbon nanorods

ABSTRACT

In this work, we exploit new sustainable carbon-based nanostructures by investigating the biomimetic pyrolysis and hydrothermal liquid crystal transfer of natural chitin nanofibrils. Chitin nanofibrils with Bouligand structure in the original crab shell are thermally carbonized to yield helical mesoporous carbon replicas. Monodisperse oleic acid-capped cobalt oxide nanoparticles are impregnated into helical pores in the carbonized membranes to generate hierarchical mesoporous Co_3O_4/C nanocomposites that are functionable as a freestanding, binder free supercapacitor. Towards colloidal chemistry of photoluminescent chitin-derived carbon nanoparticles, chitin nanorods prepared by acid hydrolysis of crab shell-extracted chitin disperse in water to form chitin liquid crystals that are used as a new carbon precursor for the carbonized transformation. Hydrophobic oleic acid-stabilized carbon nanorod colloids with optical response are primarily synthesized by hydrothermal phase transfer carbonization of chitin liquid crystals. The structural integrity of chitin nanorods can be preserved during liquid-liquid phase transformation to form carbon nanorods. The carbon anisotropic nanocolloids hydrophobically dispersed in toluene exhibit green photoluminescent emission in the visible region, which optically respond to trinitrotoluene. Our chitin inspiration paves a way to pursue further investigation of the electrochemical catalysis for the mesoporous Co_3O_4/C nanohelices and the sensing and optical coating for the photoluminescent carbon nanorod colloids.

1. Introduction

Nanoscale is an intriguing factor to study the evolution of exceptional features of materials with hierarchical structures for developing nanotechnology [1–3]. As the particle sizes of bulk materials reduce down to nanometers, new optoelectrical properties often emerge in high-surface-area nanosized objects arising from quantum confinement and surface defects [4,5]. Such behavior typically makes a material not itself as a bulk if its structure can be controlled upon synthesis at micro, nano, and atomic levels [6]. Comprehensive studies of particle size, morphological shape, functional surface, hierarchical porosity, and synthetic feasibility of nanomaterials are a means to exploit their unique properties for applications. Through nanoscale design concept, a spectacular example of nanomaterials is carbon thin films with spectacular

* Corresponding author. Department of Chemistry, University of Sciences, Hue University, 77 Nguyen Hue, Hue, 530000, Viet Nam.
** Corresponding author.
*** Corresponding author.
E-mail addresses: chauthelieutrang@gmail.com (T.T.L. Chau), tuyenvuphi@gmail.com (T.P. Vu), nguyenduccuong@hueuni.edu.vn (N.D. Cuong).

https://doi.org/10.1016/j.optmat.2021.111100
Received 18 December 2020; Received in revised form 17 March 2021; Accepted 15 April 2021
Available online 25 April 2021

transparency and mechanical flexibility instead of traditionally black color and rigidity [7]. Moreover, carbon is in a macroscopic bulk form to have black color, but typically appears the photoluminescent emission under ultraviolet light irradiation at the nanoscale [8].

Nanocarbon is a leading material for semiconductor technology owing to its electrical, thermal, chemical, and mechanical features [9,10]. Optoelectronic carbon-based nanomaterials have widely been used for many interesting applications in bioimaging, drug delivery, color display, sensors, catalysis supports, supercapacitors, and photovoltaics [11,12]. The major achievement of the nanocarbon fabrication enables the control over uniform morphology, hierarchical structure, colloidal dispersity, surface accessibility, homogeneous doping, heterojunction, and optical activity to boost the reaction performance [13]. The structure and composition of carbon materials are diverse due to the variation of their hybridization and crystallinity. They are generally in outstanding forms of fullerene, diamond, tube, graphite, and polyamorph prepared from different precursor sources employed [10]. In aspects of chemical sustainability, optoelectronic nanocarbons derived from biomass are an efficient routine to access the possibility of applications in practice [14–16]. Carbohydrates are a valuable biomass source for sustainable carbon-based micro/nanomaterials by carbonization because of its availability on earth [17].

Crabs and shrimps are the most popular seafood source in the human food chain and the food processing annually generates over 13 million tons of crustacean shell waste [18]. Chitin biopolymer is second to only cellulose, which is a main component (~15–40 wt%) in shells of crabs and shrimps [19]. As a novel biopolymer source, chitin and its derivatives are produced at around 100 billion tons per year and traditionally used in the field of biopolymer and materials chemistry at academia and industry [20]. Because of the natural abundance and economic value, it is vital to exploit new strategies of using discarded crustacean shells and extracted chitin for inspiring sustainable materials and their applications [21]. Remarkably, hierarchical structure, morphology, and composition are unique features of natural chitin nanofibrils in crustacean shells, which should be considered for research to develop applications through material biomimicry and inspiration [22]. In 1972, Bouligand Yves primarily reported a helically layered porous structure of chitin nanofibrils in some crustacean shells [23]. This structural organization leads mineralized chitin assemblies in shells to exhibit the optical anisotropy and reinforce the mechanical strength. The Bouligand's surprising discovery has inspired scientists to exploit structures of crustacean shells for mimicking functional porous carbon-based materials derived from chitin [24]. Taking advantage of chitin as a sustainable carbon semiconductor, crustacean shell-derived carbon materials were used as a supercapacitor for energy storage and the capacity of carbon electrodes could be enhanced by incorporating oxide nanoparticles (*e.g.,* cobalt oxide [25–28]). Although some porous oxide/carbon composites derived from crab shells have been inspired to design as a sustainable supercapacitors, such structural biomimicry often does not show the helical arrangement at the microscopic level.

Carbohydrate liquid crystals (LCs) are very common in nature, which could be found in lipopolysaccharides, steroidal glycosides, saponins, and cellulose [29,30]. In 1993, Revol and Marchessault early prepared chitin LCs from acid hydrolysis of natural chitin fibrils [31]. The rod-shaped chitin nanoparticle colloids obtained disperse in water to form LCs at above critical concentration. Later, scientists prepared chitin LCs to use as a nanofibril source, platform, and template to generate one-dimensional (1D) layered materials [21,32,33]. Remarkably, chitin dispersion can be used as a novel carbon precursor to create hierarchical porous carbon solids by self-assembly and carbonization [34–36]. This bioinspiration reminds us of studying chitin LCs for functional carbon-based nanocolloids with the integrity of the anisotropic shape. To the best of our knowledge, the extensive studies have mostly been focused on the transformation of chitin LCs into solid-state materials of carbon assemblies, but the carbonized transformation process of chitin LCs at liquid phase is scarcely reported.

In another work, once carbon is in particles with nanometer size domain, it generally emits photoluminescent color under light irradiation by quantum confinement effect [8]. Such optoelectronic characteristics often appear in carbon nanodots. The interesting colloidal chemistry of photoluminescent carbon nanoparticles motivates scientists to develop their applications in solar cells, sensing, photocatalysis, and bioimaging [37]. There are many ways to make photoluminescent carbon nanoparticles from different precursors [38]. Photoluminescent carbon nanoparticles derived from carbohydrates are a sustainable way recently reported by some groups [38]. Although some efforts have been devoted to the hydrothermal carbonization of carbohydrates to luminescent carbon-based nanoparticles, most of these materials are hydrophilic dot-shaped nanoparticles and natural carbohydrate macromolecules used are crude [38–43]. Natural chitin fibrils are hydrolyzed by acid to generate rod-shaped chitin nanocrystals that disperse in water to form a chitin liquid crystal [31]. However, the synthesis of hydrophobic colloidal dispersions of photoluminescent carbon anisotropic shaped nanoparticles from chitin liquid crystals is virtually unexplored.

Herein we reported the bioinspirational investigation of transformating chitin nanofibrils in discarbed crab shells into optoelectronic carbon-based nanomaterials through structural mimicry and hydrothermal carbonization. The original crab shell was pyrolyzed to obtain a mesoporous carbon replica with Bouligand-type structure after etching mineral component away by acid. Further impregnating uniform cobalt oxide nanoparticles onto biomimetic mesoporous carbonized networks afforded cobalt oxide/carbon composite replicas that can function as a binder free supercapacitor. Alternatively, the crab shell was purified to extract chitin that hydrolyzed by acid to obtain nanorod-shaped chitin liquid crystals. The chitin liquid crystals were used as a new anisotropic precursor to synthesize oleic acid-stabilized carbon nanorod colloids with shape replication, hydrophobic surface, and photoluminescent response by hydrothermal phase transfer of chitin from water into toluene.

2. Chemical experiments

Chemicals. Crab shells were obtained from discarded sources of seafood processing. Oleic acid, cobalt nitrate, potassium oleate, trinitrotoluene were purchased from Sigma-Aldrich and used as received. Toluene, hydrochloric acid, sodium hydroxide, hydrogen peroxide, and ethanol were obtained from standard suppliers.

Hierarchical mesoporous Co_3O_4/C nanocomposites inspired by crab shells. The pyrolysis of chitin was accomplished under nitrogen by heating original crab shells to 100 °C at 5 °C min^{-1} for 4 h and up to 600 °C at 5 °C min^{-1} for 8 h to generate mineralized carbonaceous composites. The calcium carbonate component in the carbonized composites was removed by treating the sample with 1 M HCl at room temperature for 24 h. Hierarchical mesoporous carbon nanomaterials were obtained after filtering, washing with copious water, and drying at ambient conditions.

For the preparation of oleic acid-capped Co_3O_4 nanocrystal colloids, 10 mL ethanol solution containing 3 mg potassium oleate was added to a 20 mL toluene/2 mL oleic acid solution and then mixed with 20 mL of Co $(NO_3)_2$ aqueous solution (0.08 M, 1.6 mmol) to form a two-phase mixture, in which the oleate anions disperse into the oil phase. The biphasic mixture was transferred to a teflon-lined stainless steel autoclave and heated at 180 °C for 24 h to proceed the hydrothermal reaction. The reaction mixture obtained after hydrothermal treatment remained the two phases, where the dark brown nanocrystal solution in the upper toluene phase was separated from the lower water phase and precipitated by excessively adding ethanol. The purified nanocrystals were collected by centrifugation and redispersed in toluene. The precipitation-redispersion process was repeated for two times to purify hydrophobic oleic acid-capped Co_3O_4 nanocrystal colloids.

For the preparation of Co_3O_4/C nanocomposites, 1.0 mL of oleic

acid-capped cobalt oxide toluene dispersion was dropcast onto porous carbon membranes (~250 mg) and let them dry at ambient conditions for 10 min. This loading and drying process was repeated for three times to infiltrate the sufficient amount of the oxide nanoparticles within the pores of the carbon membranes. To increase interfacial interaction between active cobalt oxide nanoparticle deposits and carbon supports, the resulting composites were pyrolyzed at 350 °C under nitrogen for 2 h to generate freestanding Co_3O_4/C composite films with hierarchical mesoporous structure.

Oleic acid-capped carbon nanorod colloids hydrophobically dispersed in toluene derived from chitin liquid crystals. For the preparation of nanorod-shaped chitin liquid crystals, cleaned crab shells (~50 g) were treated with a NaOH aqueous solution (5 wt%, 1000 mL) at 90 °C for 6 h to remove protein and then treated with an HCl aqueous solution (7%, 1000 mL) twice at room temperature for 24 h to remove minerals. The deproteinized and decalcified chitin samples were washed with copious water and then treated with an H_2O_2 aqueous solution (5 vol%, 1000 mL) at 90 °C for 1 h to bleach organic pigments. To prepare chitin nanocrystals, the purified chitin samples (~5 g) were treated with a NaOH aqueous solution (33 wt%, 80 mL) at 90 °C for 2 h for the surface deacetylation of amino groups. The deacetylated chitin samples were collected and neutralized by washing thoroughly with water, and then treated with an HCl aqueous solution (4 M, 100 mL) at 104 °C for 18 h to hydrolyze chitin nanofibrils to rod-shaped chitin nanocrystals. Because organic pigments in the crab shell were oxidized during acid hydrolysis to form dark-brown reaction mixtures. These pigments in the reaction mixture were oxidized by H_2O_2 (30%, 25 mL) at 90 °C for 30 min to obtain cloudy chitin solutions [44]. After acid hydrolysis, the reaction mixtures were diluted with 100 mL water and then centrifuged to remove soluble chitin species. This purification was repeated for three times to obtain a cloudy chitin aqueous suspension. The chitin nanocrystal colloids were adjusted to the concentration of ~6.6 wt% and the pH value to ~4 to form a stable chitin aqueous suspension [33].

For the preparation of hydrophobic oleic acid-capped carbon nanorods, a 5 mL portion of chitin aqueous solution (6.6 wt%, pH~4) was mixed with 4 mL toluene containing 1 mL oleic acid under stirring at room temperature for 1 h. The two-phase mixture was poured into a teflon-lined stainless steel autoclave, which seated and heated at 180 °C for 24 h. After hydrothermal treatment, the upper phase changed to dark brown in color, which was clearly separated from the lower phase by funnel. The collected upper water phase was purified by centrifugation to obtain a homogeneous colloidal dispersion showing green photoluminescent colors under UV light excitation.

Structural analysis. Powder X-ray diffraction (PXRD) patterns of the samples were recorded on an Advance Bruker D8 X-ray diffractometer. Scanning electron microscopy (SEM) images of the samples were obtained on a JSM-5300LV electron microscope. Samples were prepared by attaching them to aluminum stubs using double-sided adhesive tape and sputter coating with Au (5 nm). Transmission electron microscopy (TEM) images of the samples were obtained on a JEOL-JEM 1010 electron microscope. Infrared (IR) spectroscopy was obtained on neat samples using a IR-Prestige-21 spectrometer. Zeta potentials of the dilute chitin solutions (0.001 wt%, pH~4) were obtained using an Anton Paar Litesizer 500. Thermogravimetric analysis (TGA) of the samples (~10 mg) was conducted at the heating rate of 10 °C min^{-1} under air and/or nitrogen atmosphere from RT to 800 °C using a Labsys TG/DSCSE-TARAM thermogravimetric analyzer. Polarized optical microscopy (POM) was performed on an Olympus BX40 microscope. The UV–Vis adsorption spectroscopy of the solution was recorded using a Jasco V-630 spectrophotometer. Photoluminescence spectroscopy was obtained on a Hitachi F4500 fluorimeter. Raman spectroscopy was performed using a SpectraCode model RP-1 spectrometer with a 785 nm diode laser excitation. Nitrogen adsorption-desorption isotherms (US) were obtained using a Micromeritics at 77 K and the samples (~120 mg) were degassed at 150 °C in vacuum for 4 h before measurements. Cyclic voltammetry measurements were performed with a two-electrode configuration using a Brinkmann PGSTAT12 Autolab potentiostat. The freestanding films were weighed and soaked in a 1 M KCl aqueous solution for at least 24 h. Two pieces of symmetrical films, Whatman filter paper piece, and 1 M KCl were used as electrodes, separator, and electrolyte, respectively. Stainless-steel collectors sandwiched two films with a filter paper separator, which were placed in a Swagelok two-electrode cell.

3. Results and discussion

In 1970s, Bouligand Yuves early reported the twisted plywood arrangement of chitin nanofibrils in some crusteacean shells, resembling a cholesteric mesophase of liquid crystals [23]. In 1993, Revol and Marchessault pioneered the synthesis of chitin liquid crystals by acid hydrolysis of chitin fibrils [31]. Chitin nanoparticles in liquid crystals could be a novel carbon precursor to innovate optoelectronically carbonized materials with anisotropically structured features [34]. In aspect of the natural evolution, our current work deeply considered the novelty of the twisted fibrous organization and chitin liquid crystal-derived carbon in abundantly discarded crab shells to inspire new types of optoelectronical carbon-based nanostructures through biomimetic pyrolysis and hydrothermal phase transfer.

To inspire carbon nanomaterials with the Bouligand-type structure, the original crab shell was pyrolyzed at 600 °C under nitrogen to generate $CaCO_3$/C composites. The carbonized shell was treated with a 1 M HCl solution at room temperature to dissolve the $CaCO_3$ component and yielded a black carbon replica (Fig. S1a). The obtained carbon materials originally retained the macroscopic shell features with thermal shrinkage. Scanning electron microscopy (SEM) images (Fig. 1a) of the carbon replica show two helical systems: one is carbon nanofibrils twisted around helical axis to form a twisting layer structure and another is helicoidal canal-like microchannels (see more detail in their decorated composites in Fig. 2). Both the helical systems integrated together in a highly complicated but sophisticated way to form a twisted porous framework in the sustainable carbon membrane. Structural analyses showed the carbon material is amorphous and mesoporous as evidenced by Powder X-ray diffraction (PXRD), Raman spectroscopy, and nitrogen adsorption-desorption isotherms (Fig. 4) [45–47]. The gas adsorption-desorption isotherms measurement showed a type-IV isotherm with type-H2 hysteresis to reveal mesoporous structure in the crab shell-derived carbon materials. The carbon material has a BET surface area of ~800 m^2 g^{-1} and pore size of ~12 nm associated to the presence of nanosized void spaces between carbonized chitin nanofibrils (Fig. 4d). The structural imprint of the large porous networks could lead the macroscopic helical carbon films to be a novel platform for additive deposits to develop functional composites with unique electrochemical property.

Cobalt oxide nanoparticles are a p-type semiconductor with oxygen vacancies and other native defects, which are useful for electrochemical and optoelectronic devices [48,49]. Chemically stabilized carbon networks can host electrochemically active cobalt oxide at the nanoscale to boost the reaction performance by the influence of interfacial effects. The engineering of hierarchical porosity in cobalt oxide/carbon nanocomposite semiconductors is also key to improve the reactivity by diffusion of reactants inside pores [50]. Therefore, sustainable cobalt oxide/carbon nanocomposites inspired by crab shells have a great potential in applications of energy storage, catalysts, catalytic substrates, and sensors [26,51–53]. To prove such heterojunction, we impregnated cobalt oxide nanoparticles into the helical porous carbon films and their enhanced electrochemical properties were evaluated for supercapacitor. Hydrothermal two-phase synthesis was used to synthesize oleic acid-capped Co_3O_4 nanoparticles with the size of ~5–10 nm (Fig. 1b and c) [54]. The oleic acid-capped cobalt oxide nanoparticles monodispersed in toluene to form a colloidal solution that gently dropcasted on the porous carbon films. The toluene solvent quickly evaporated off to diffuse the cobalt oxide nanoparticles into pores through carbon film.

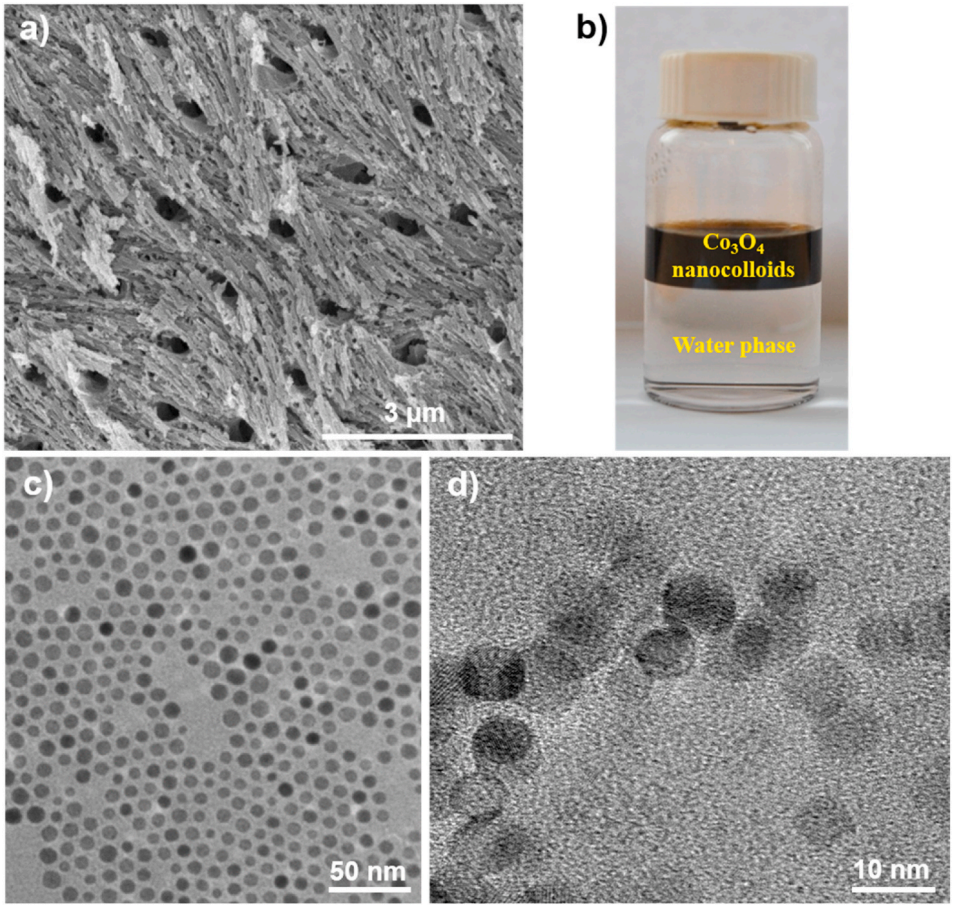

Fig. 1. (a) SEM image of crab shell-derived carbon nanomaterials with twisted Bouligand structure and TEM image (c) and HRTEM image (d) of oleic acid-capped Co_3O_4 nanocrystals prepared by hydrothermal two-phase transfer shown in photo (b).

The nanoparticle dropcast was repeated for three times to increase the loading of the oxide nanoparticles, and consequently a homogeneous Co_3O_4/C composite film was obtained (Fig. 2a). The resulting composites were heated at 350 °C for 2 h to pyrolyse the oleic acid capping agent adsorbed on the materials and thus increased cobalt oxide-carbon interactions in the composite films.

Scanning electron microscopy (SEM) images (Fig. 2b–d) show that the cobalt oxide nanoparticles fully decorated onto the helical porous carbon networks. The deposition is mostly homogeneous through Bouligand structure, where the individual oxide nanoparticles directly attached to the carbon nanofibrils and others aggregated into larger ones confined in the helical canal-like macrochannels. Upon impregnation, the cobalt oxide nanoparticle colloids first had a tendency to homogeneously insert into the mesoporous arrays between carbon nanofibrils. Once this colloidal deposition was full, the oxide nanoparticles located on walls of the macroporous canals and on surfaces of the carbon films. Upon pyrolysis in nitrogen, the carbon structure further shrunk to lock the deposited oxide nanoparticles within the mesoporous arrays of carbon nanofibrils, forming uniform cobalt oxide@carbon hybrid nanofibrils. The oxide nanoparticles placed on the surfaces of the macroporous channels and films tended to agglomerate to minimize their surface energy and as a consequence of forming the larger oxide nanoparticle aggregates with the sizes up to several micrometers. Therefore, the structural shrinkage and agglomeration by further pyrolysis after deposition caused the oxide nanoparticles to be tightly attached onto the pores of the carbon frameworks. Transmission electron microscopy (TEM) images (Fig. 3) were used to further analyze the Co_3O_4/C structure. It can be observed ~10–20 nm sized nanoparticles heterogeneously inserted into the mesoporous carbon nanofibril assemblies with helically layered structure, which is consistent with the SEM results. Also note that the further pyrolysis of the composites obtained after deposition led to the growth of the cobalt oxide nanoparticles onto the carbon matrix. As a result, the sizes of the cobalt oxide nanoparticles deposited in the porous carbon networks in the final product are larger than those of the parent nanoparticle colloids. The composite also remained nanosized spaces between the Co_3O_4/C hybrid nanofibrils to indicate the presence of mesopores, consisting with the nitrogen sorption data (Fig. 4d). These electron microscopy examinations fully prove the original conservation of the twisted Bouligand arrangement in the Co_3O_4/C nanocomposites obtained after thermal pyrolysis of the natural crab shells followed by chemical purification and nanoparticle deposition. The impregnation and heating did not disrupt the cubic structure of the Co_3O_4 nanocrystals deposited onto the porous carbon matrix, as evidenced by PXRD in Fig. 4a [55]. Thermogravimetic analysis (TGA) confirmed the cobalt oxide deposit to be ~20 wt% in the carbon support (Fig. 4c). Nitrogen sorption isotherms show the composite still remained the mesopororous structure with the surface area of ~250 $m^2\ g^{-1}$ (Fig. 4d). Through structural mimicry, this is the first experiment of inspiring the crab shell-derived carbon Bouligand structures impregnated with the uniform oxide nanoparticles.

The cobalt oxide nanoparticles known as an outstanding catalyst combined with the carbon semiconductor support, which lead the hierarchical mesoporous nanocomposites to hold the potential for electrochemical catalysis, gas sensing, and supercapacitor applications. We evaluated the electrochemical properties of the hierarchical porous Co_3O_4/C nanocomposites with an eye to their potential use in supercapacitor electrodes using cyclic voltammetry (CV) in Fig. 4e and f. The freestanding Co_3O_4/C composite films were directly used as electrodes

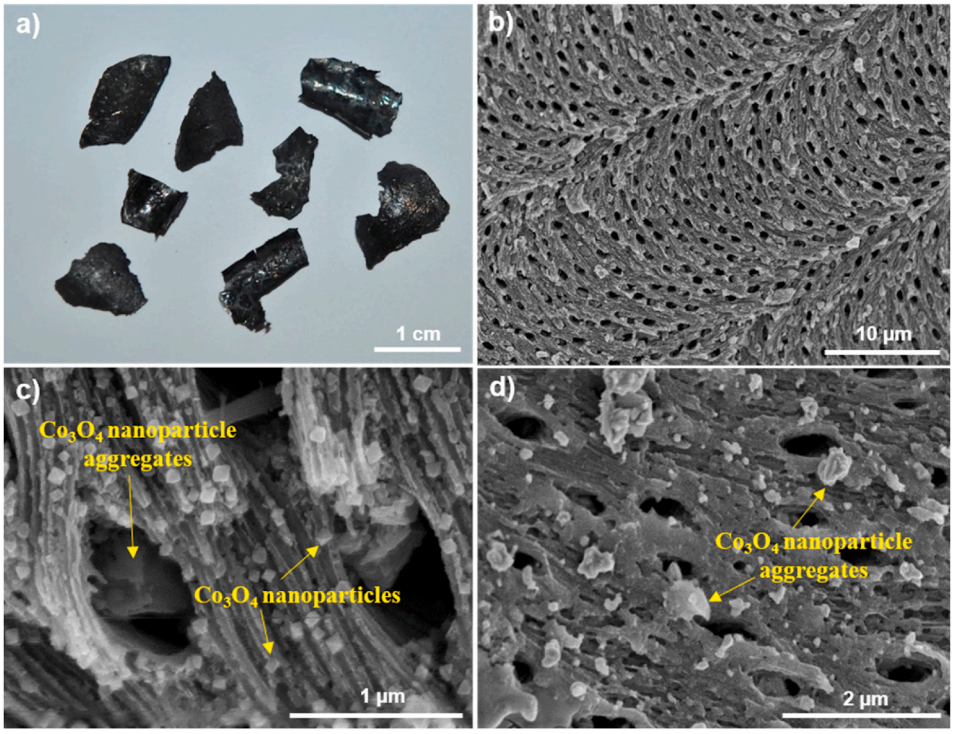

Fig. 2. Biomimetic pyrolysis carbonization of chitin nanofibrils with Bouligand-type structure in abundantly discarded crab shell to hierarchical mesoporous carbon replica impregnated with cobalt oxide nanoparticles. a) Photo of freestanding Co_3O_4/C composites, SEM images of cross section of Co_3O_4/C composite film at (b) low and (c) high magnifications, and d) SEM image of top view of Co_3O_4/C composite film.

in a binder free two-electrode symmetric supercapacitor and 1 M KCl solution was used as an electrolyte. The CV of the Co_3O_4/C shows a nearly rectangular shape at a scan rate of 10 mV s^{-1} with no noticeable redox peaks, suggesting a highly capacitive behavior with good ion response. This feature also indicates the charge-discharge process occurring at the pseudo constant rate over the applied cycle. The Co_3O_4/C composite shows a specific capacitance (C_s) of ~200 F g^{-1} that is higher than that of the parent carbon sample (~170 F g^{-1}). This assumes that the Co_3O_4 nanodeposites improved the faradaic capacitance of the carbon support, which could result in contributing to charge storage through a pseudo-capacitve mechanism. The carbon matrix supported the cobalt oxide nanoparticles to minimize their volume expansion/contraction, which thus may exhibit synergetic electrochemical properties as well. Beyond this, we believe that the uniqueness of the nanoscale helicity and porosity at the microscopic level endows the helical cobalt oxide/carbon composites with chiral functionality to further investigate their interesting other applications in chiral separation, chiral molecule absorption, and/or chiral catalysis [56–59].

Beyond solid-state materials as the hierarchical porous carbon films, we motivated to inspire the colloidal chemistry of shape-controlled carbon nanoparticles from crab shell-derived chitin liquid crystals. To pursue this concept, we turned the natural chitin fibrils to nanocrystalline chitin colloids by acid hydrolysis reported by Marchessault and Revol [31]. Hydrolyzed chitin rod-shaped nanocrystals typically disperse in water to form a liquid crystal system. Our goal is to investigate the conversion of chitin nanoparticles in liquid crystals to colloidal carbon nanoparticles with the integrity of the anisotropic shape. Rather than aqueous media, we preferred to achieve hydrophobic carbon nanocolloids with optoelectronic response to value their potential uses.

We first set out to synthesize chitin liquid crystals prepared from the discarded crab shell and used them as a new precursor to make hydrophobic carbon nanocolloids with controllable shape. The cleaned crustacean shells were sequentially deproteinized, demineralized, and depigmented to purify chitin pieces. The extracted chitin nanofibrils were treated in a hot concentrated alkali solution and the resulting sample was hydrolyzed in a 4 M HCl aqueous solution at 104 °C to form chitin nanocrystals. The chitin nanocrystal product was collected from the reaction mixture by centrifugation and then dispersed in deionized water under sonication to form a homogeneous chitin suspension. This colloidal suspension is an anisotropic chitin liquid crystal at the critical concentration of 6.6 wt% (Fig. 5a-left).

TEM images (Fig. 5b,e) of the prepared chitin aqueous dispersion show that chitin nanocrystals are discrete rod-shaped nanoparticles with the diameter of ~5–10 nm and the length of ~300–500 nm. These sizes are considerably smaller than those of the purified chitin nanofibrils, proving that rod-shaped chitin nanocrystals are hydrolyzed anisotropic fragments of the natural chitin nanofibrils. POM examination of the chitin aqueous dispersion showed anisotropic birefringent textures characteristic of a nematically layered liquid crystal (Fig. 5c). These experimental results confirm that the defragmentation of the purified natural chitin nanofibrils under these identical reaction conditions recovered well-defined chitin nanorod colloids that can disperse in water to form an anisotropic chitin liquid crystal [31,60].

Recent progress has shown that the hydrothermal reaction is an efficient method to break down carbohydrates to form carbon nanoparticles upon carbonization conditions in aqueous media. We applied a similar experiment for chitin nanocrystals to proceed the hydrothermal carbonization. We found that the hydrothermal treatment of chitin aqueous suspension (6.6 wt%, pH~4) with liquid-crystalline features at 180 °C often form carbonized gels rather than dispersed nanocolloids. To avoid this issue, we used 1.0 wt% chitin aqueous dispersion diluted from 6.6 wt% chitin liquid crystals and the hydrothermal treatment typically generated photoluminescent carbon nanocolloids dispersed in water (Figure S8). However, the carbon colloids are nanodots instead of the original nanorods from the parent chitin nanocrystals, which are mostly similar to previously reported carbon nanodots hydrothermally derived from carbohydrates [61,62]. In water, the decomposition of chitin nanocrystals can be accelerated under hydrothermal carbonization to result in forming carbon nanodots. This behavior could be

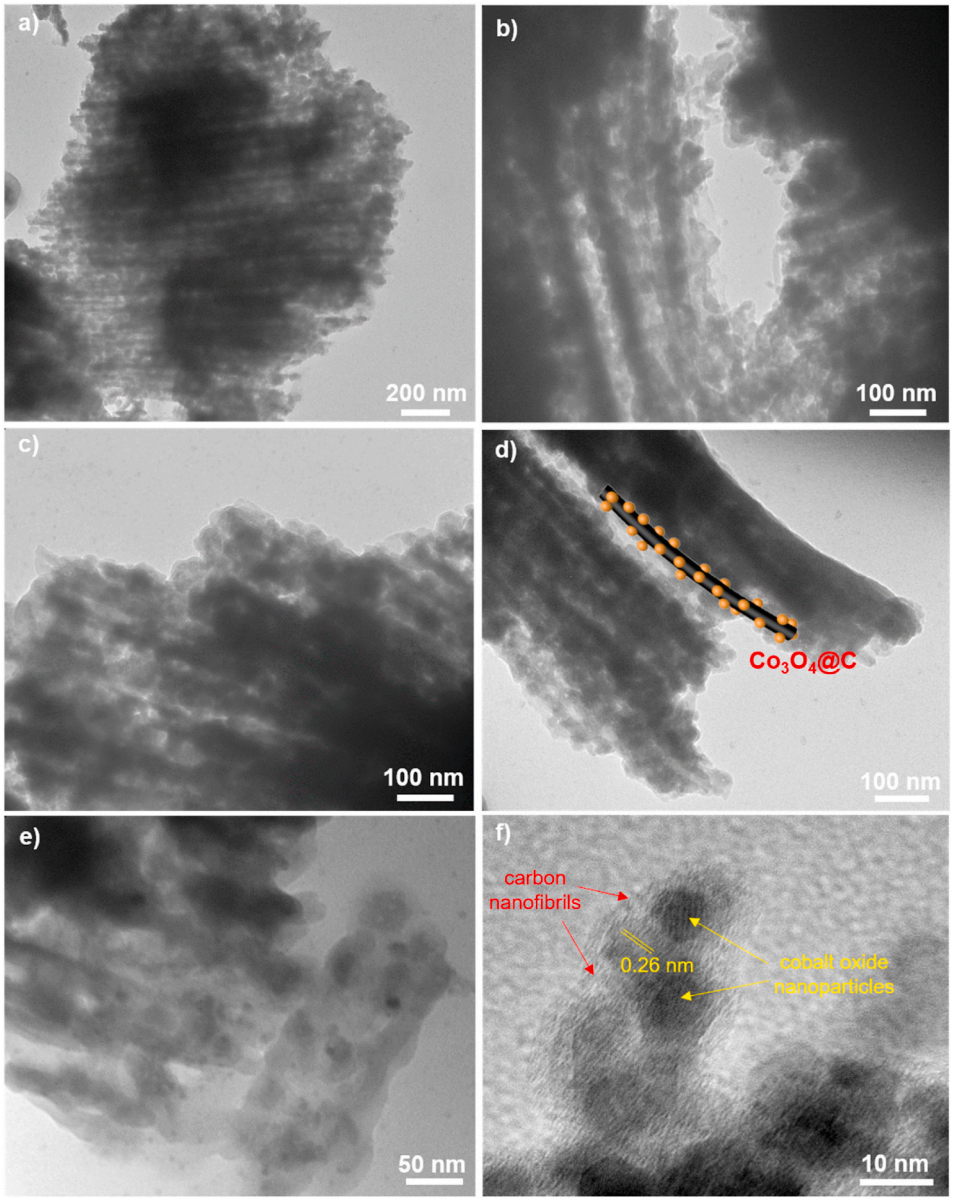

Fig. 3. Heterogeneous decoration of cobalt oxide nanoparticles onto carbon nanofibrils in Bouligand structured films: TEM images of cobalt oxide/carbon composites and HRTEM image in (f) clearly reveals cobalt oxide nanocrystals with a lattice space of 0.26 nm decorated onto an amorphous carbon nanofibril matrix, thus leading to the formation of a metal oxide@carbon nanohybrid composite.

minimized by using a non-polar solvent to proceed the hydrothermal carbonization of nanorod-shaped chitin liquid crystals, and consequently colloidal carbon nanorods might be yielded. To deal with this motivation, we investigated a hydrothermal two-phase transfer approach to enable the conversion of chitin liquid crystals to colloidal carbon nanorods.

Chemically, the hydrolysis of natural chitin yielded chitin nanocrystals with exposed surface amine groups. Elemental analyses confirmed 43.70 wt% carbon and 6.30 wt% nitrogen in the prepared chitin nanocrystals, assuming that about 70% of the primary amine groups present on chitin nanorods [63]. In acidic media, these exposed amine groups are protonated to turn chitin nanocrystals to anisotropic nanocolloids with positively charged surface. This can be convinced by zeta potential (ζ) measurement of the chitin aqueous suspension to evaluate the ζ value of approximately +13 eV. The positively charged surface of highly dispersed, well-defined chitin nanorods reminded us a possible way of the phase transfer of the amphiphilic liquid crystals into a hydrophobic oil solution for the material development by charged and/or coordinated interactions [64].

Central for our approach is the use of the hydrophobically coordinated ligand of oleic acid to interact with positively charged hydrophilic chitin nanorods to possibly form intermediate complexes. These interactions may occur at water-toluene interfaces to allow the resulting complexes to proceed the phase transfer under reaction conditions to create new materials with the structural integrity of the anisotropic shape of chitin nanorods.

We set out to make experiments of the hydrothermal phase transfer of chitin liquid crystals into a non-polar solvent in the assistance of oleic acid. In a typical synthesis, a two-phase reaction system of aqueous liquid crystal and oil was designed and proceeded hydrothermal treatment. We used directly pure chitin liquid crystals (6.6 wt%, pH~4) as a hydrophilic aqueous phase. The hydrophobic oil phase is a mixture of toluene solvent and oleic acid simultaneously as a phase transferring agent and a capping agent. These two phases were mixed together to form a homogeneously phase-separated system, where the upper phase is the oleic acid-toluene solution and the bottom phase is the chitin

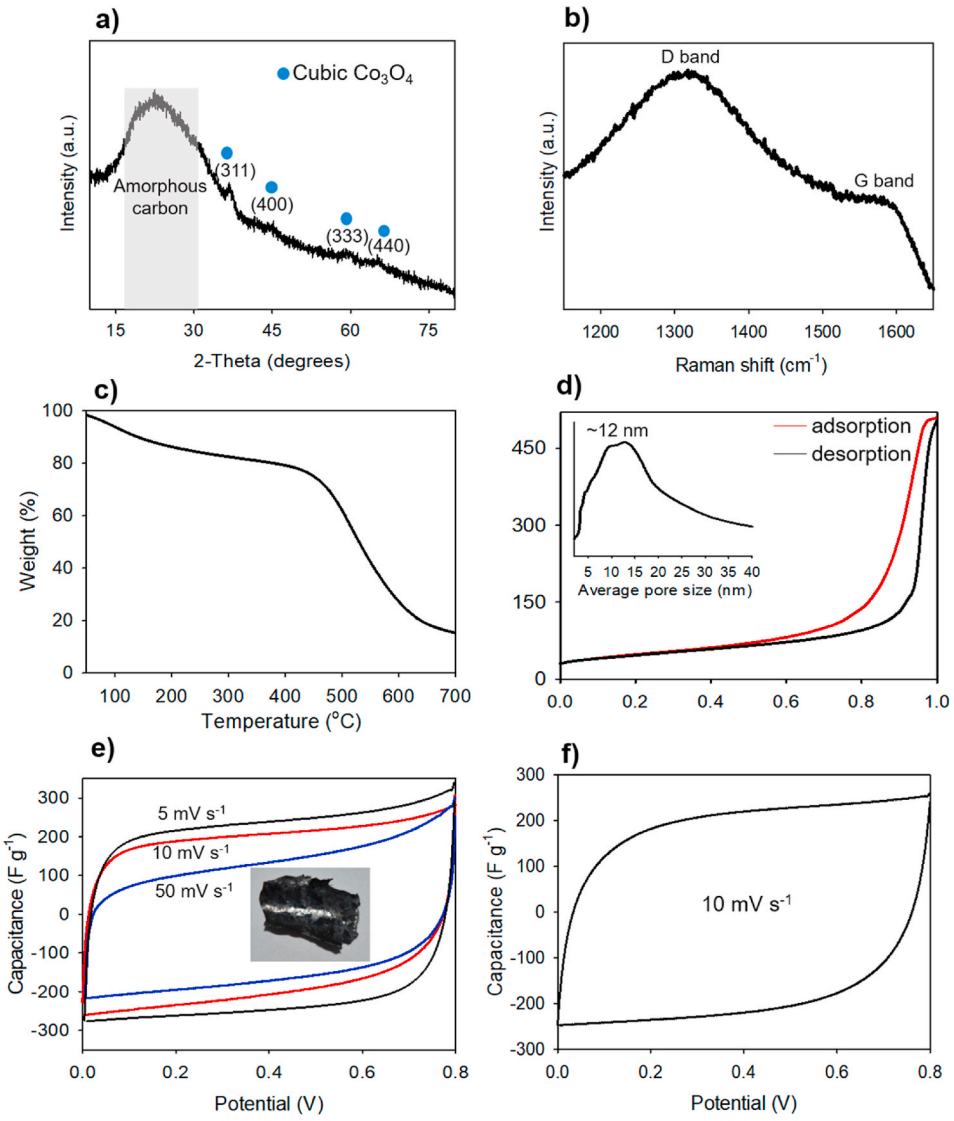

Fig. 4. Structural analysis and electrochemical property of hierarchical porous Co_3O_4/C composites. a) PXRD pattern of Co_3O_4/C composite, b) Raman spectrum of Co_3O_4/C composite, c) TGA profile of Co_3O_4/C composite running at 10 °C min^{-1} under air atmosphere, d) Nitrogen adsorption-desorption isotherms (inset is a Brunauer-Joyner-Halenda (BJH) pore size distribution) of Co_3O_4/C composite, and Cyclic voltammetry curves of (e) cobalt oxide/carbon composite films vs (f) pure carbon films in 1 M KCl electrolyte to evaluate their electrochemical property.

aqueous suspension (Fig. 5d-left). This biphasic system was used to investigate the phase transfer of chitin nanorods into toluene under hydrothermal treatment.

Due to possible interactions between chitin nanocrystals and oleic acid under mixing, we investigated the phase transfer of chitin nanocrystals at ambient conditions before thermal reaction. Under stirring for 1 d at room temperature, the distribution of chitin nanocrystals in the toluene phase was examined by optical and electron microscopies. Optical microscope observation showed some aggregated crystals with birefringent textures in the oil phase (Fig. 5f). TEM images (Fig. 5e) confirm the presence of some nanorods in the oil phase and they largely distribute in the interface. These nanorods have size and shape features resembling those of chitin nanorods in liquid crystals, indicating that the nanocomponent distributed through the oil phase is chitin nanocrystals. These results assume oleic acid/chitin interactions occurring at the interface at room temperature, leading some chitin nanorods in the aqueous phase to transfer into the toluene phase.

The nanochitin phase transfer encouraged us to investigate the hydrothermal carbonization of the anisotropic chitin crystals in the oleic acid/toluene phase (Scheme 1). Predictably, the temperature elevation accelerates the phase transfer of chitin nanocrystals to enable the achievement of functional carbonized nanocomponents dispersed in a non-polar solvent. Hence, our initial experiments were performed by pouring the two-phase mixture into an autoclave and heating it at 180 °C for 20 h. As expected, after hydrothermal treatment the reaction mixture changed to brown in color and the two-phase separation was maintained as original (Fig. 6b). Remarkably, the upper phase is a homogeneous, transparent brown solution, assuming that the phase transfer and hydrothermal carbonization of chitin nanorods simultaneously occurred by heating. Impressively, the upper phase appears a strong green luminescent color when viewed the hydrothermal two-phase mixture under UV light (Fig. 6c). Since carbon is semiconductor that typically exhibits photoluminescence at the nanoscale. This optical visualization reflects the generation of semiconducting carbon nanoparticles from chitin liquid crystals.

The upper phase was collected from the hydrothermal two-phase mixture and purified to investigate the structural features of the resulting materials. Surprisingly, the luminescent toluene solution obtained after reactions mainly contains individual nanorods with monodispersity and good distribution as evidenced by TEM images in Fig. 7a–d. No other shapes of the resulting nanoparticles could be observed in the sample. These hydrophobic nanorods have the average size of ~4–6 nm in diameter and ~100–300 nm in length, which are a little smaller than those of the pristine chitin nanorods. This result suggests that the synthetic experiment yielded carbonized nanorods from the chitin nanorods with thermal shrinkage.

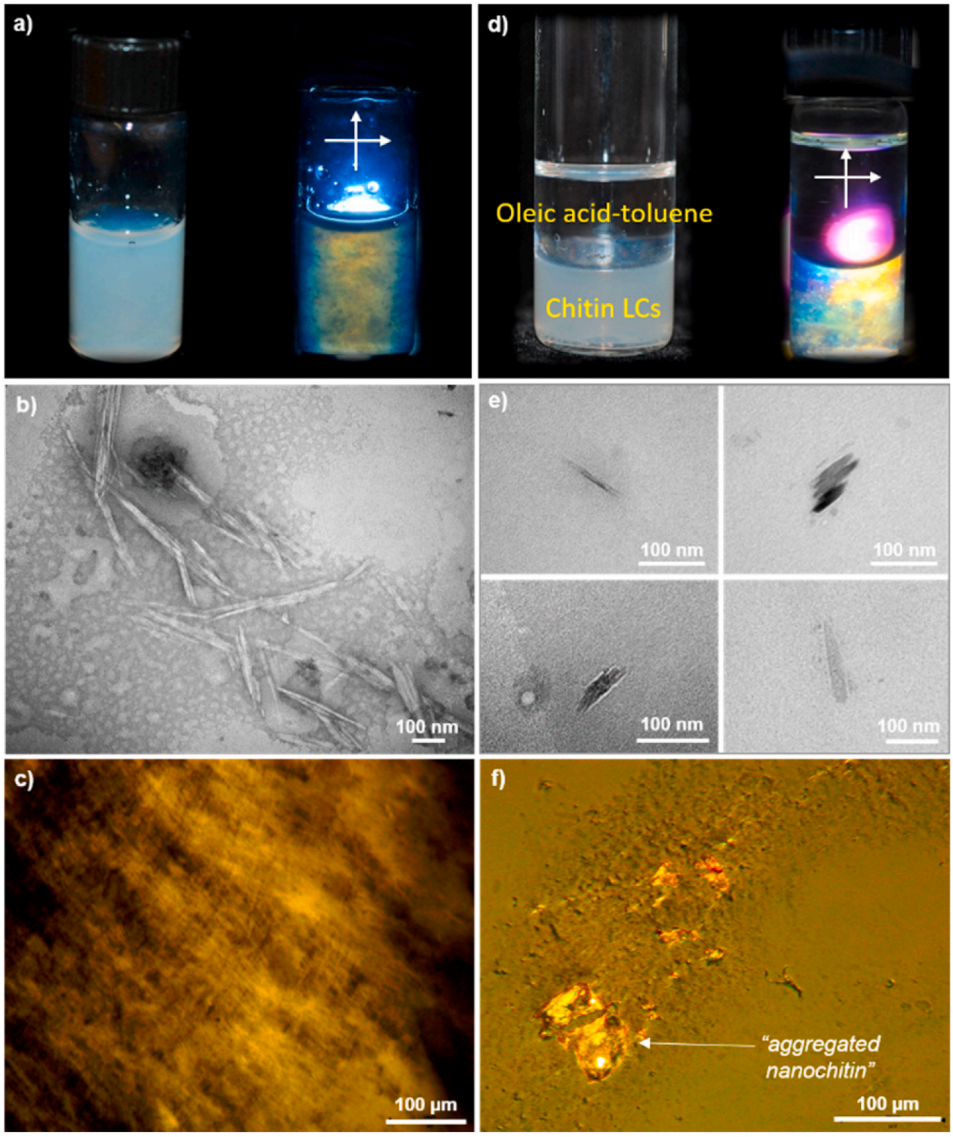

Fig. 5. Rational design of a hydrothermal biphasic transfer system of chitin liquid crystals as a water phase and oleic acid/toluene as an oil phase for the sustainable synthesis of hydrophobic carbon nanorod colloids. (a) Photos of chitin liquid crystals (6.6 wt%, pH~4) viewed under visible light (left) and under circularly polarized light (right), (b) TEM image of chitin nanorods in liquid crystals, (c) POM image of chitin liquid crystals, (d) Two-phase system of chitin liquid crystals (lower) and oleic acid/toluene (upper) viewed under visible light (left) and under circularly polarized light (right), (e) TEM images of chitin nanocrystals partially dispersed in the oil phase before hydrothermal treatment, (f) POM image of the oil phase containing some chitin from the initial phase transfer.

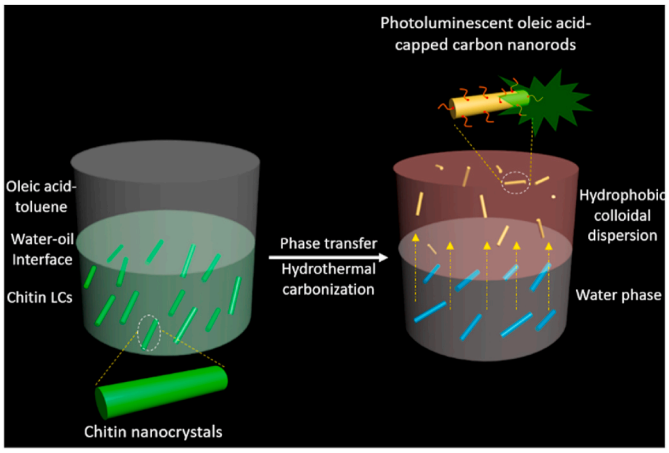

Scheme 1. Schematic of the phase transfer of chitin liquid crystals in water into photoluminescent carbon nanorods in toluene during hydrothermal carbonization.

The hydrophobic stabilization of the colloids in toluene can be a result of the passive surface of the carbonized nanorods by oleic acid. The hydrothermal carbonization of carbohydrate macromolecules often affords nanocarbon and some soluble organic intermediates that both emit photoluminescent colors under UV light excitation. Hence, to determine structural properties of main products derived from nanochitin by hydrothermal phase transfer carbonization, we purified the luminescent colloidal solution in the upper phase to selectively collect the carbonized nanorods. Typically, the colloidal dispersion was concentrated up by drying off toluene and then added ethanol to precipitate the carbonized nanorods out of the solution. The precipitate was collected by centrifugation, washed with ethanol, and dried in air to obtain a brown powder with lightweight characteristics. Eventually, the purified powder was quickly redispersed in toluene to form a brown colloidal solution with the retention of homogeneity and transparency (Fig. 6e). This dispersion mostly remains the brilliant green photoluminescence of the pristine sample under UV light excitation at the same wavelength, indicating that the emission mainly arises from the carbonized nanorods (Fig. 6f).

The purified photoluminescent carbon nanorods were characterized using a variety of analytical techniques. Infrared (IR) spectroscopy (Fig. 7h) shows that the carbon nanorod has stretching bands of alkyl groups at ~2850-2930 cm^{-1} that resemble those of free oleic acid [65].

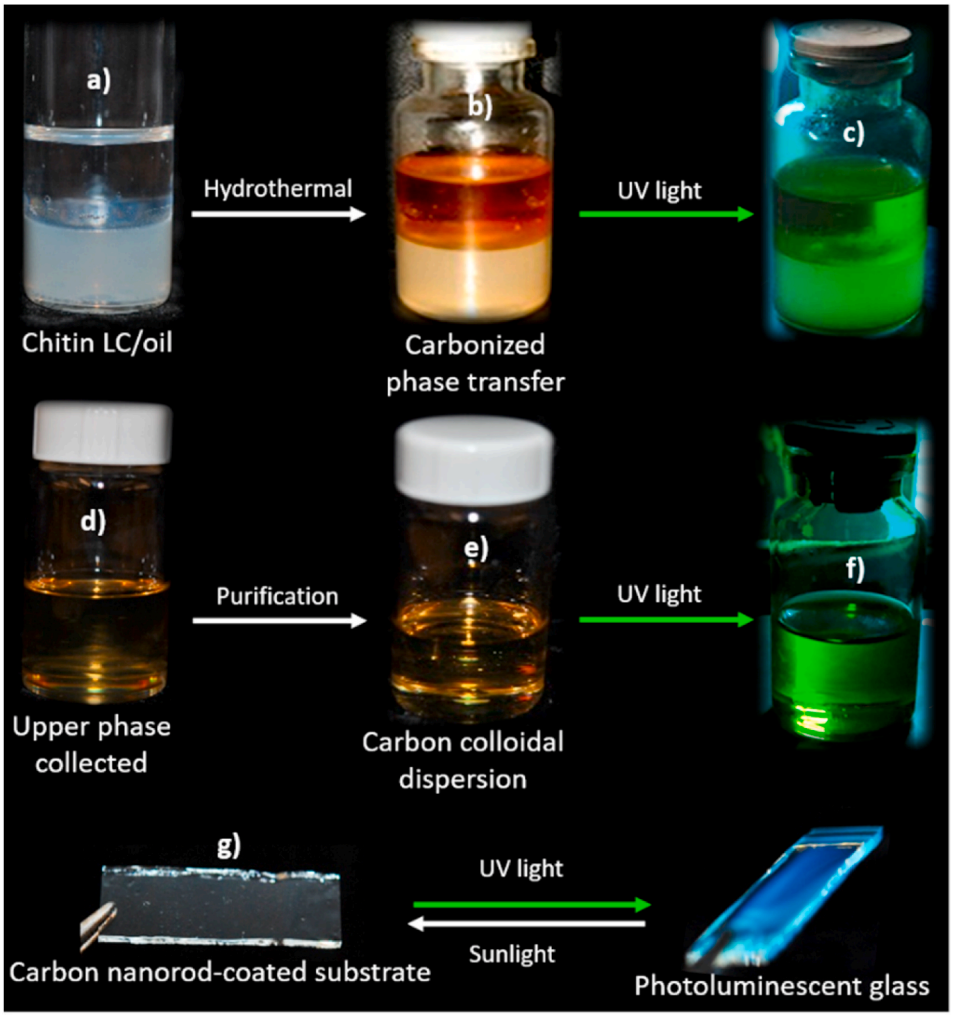

Fig. 6. Hydrothermal phase transfer of chitin liquid crystals into luminescent oleic acid-capped carbon nanorods in toluene. Photos of two-phase system of chitin liquid crystals and oleic acid/toluene (a) before and (b) after hydrothermal carbonization. (c) Photo of hydrothermally carbonized two-phase system viewed under UV light irradiation, (d) Photo of carbonized nanorod-contained oil phase separated from the reaction mixture, (e) Photo of purified carbon nanorod powder colloids redispersed in toluene, (f) Photo of purified carbon colloidal dispersion viewed under UV light irradiation, (g) Photos of layer coating of the as-prepared carbon nanorod dispersion on silica glass viewed under visible light and UV light irradiation.

However, IR bands at ~1530-1560 cm^{-1} attributed to asymmetric and symmetric C–O stretching modes of carboxylate groups of oleic acid were observed in the carbon nanorods. Free oleic acid has an IR band at ~1710 cm^{-1} ascribed to the vibration of free –COOH, which is absent in the carbon sample [65]. This result verifies that oleic acid capped on the carbon nanorod's surface. The stability of oleic acid on the carbon nanorods makes them hydrophobic, leading to the monodispersity in toluene. PXRD pattern (Fig. 7f) of the carbonized nanorods shows a broad hump at ~23° characteristic of amorphous graphite structure that is different from the crystallinity of chitin nanorods [66]. Raman spectrum (Fig. 7g) of the carbonized nanorods shows a D band at ~1340 cm^{-1} and a G band at ~1560 cm^{-1} characteristic of amorphous carbon structure [66]. Elemental analysis confirmed that the carbonized nanorod contains 1.60 wt% nitrogen compared with 6.30 wt% nitrogen in the chitin nanorods. The high percentage of carbon in the carbonized nanorods versus the chitin nanorods likely results from the carbohydrate carbonization. The presence of nitrogen in the carbonized nanorods proves that the synthesized product is nitrogen-doped carbon [66]. Altogether it can lead to a conclusion that the luminescent carbonized nanorod colloids are made of oleic acid-capped nanocarbon polymorph.

The oleic acid-capped carbon nanorods were characterized by optical spectroscopy. UV–Vis spectra (Fig. 7e) of the oleic acid-capped carbon nanorods homogeneously dispersed in toluene show a pronounced absorbance shoulder centered around 250–320 nm. Photoluminescence spectra (Fig. 7e) of this sample show a strong, broad emission with a maximum peak at 420 nm. This wavelength range of the maximum emission is consistent with the green luminescent color of the colloidal dispersion observed by naked eyes. These results confirm that the oleic acid-capped carbon nanorods derived from chitin liquid crystals are hydrophobic semiconductor colloids exhibiting the efficient luminescent property. We also found that the carbon nanorod colloids sufficiently interact with a trace amount of trinitrotoluene (TNT) to quickly quench their photoluminescent signal as evidenced in Fig. 7e. This electrochemical response reflects that the photoluminescent carbon nanorods could be designed into optical probes and sensors.

The shape resemblance of the oleic acid-capped carbon nanorods and the chitin nanorods fully proves the concurrence of the transfer phase and hydrothermal carbonization. This result may predict that oleic acid first interacts with chitin nanorods and/or carbonized nanorods at the toluene-water interface, which later transfers carbon nanorods stabilized by oleic acid into the toluene phase upon hydrothermal treatment. We found that oleic acid plays a key role in forming the homogeneous non-polar dispersion of the luminescent carbon nanorods by simultaneously being as a phase transferring agent and as a colloidal stabilizer. The phase transfer of the nanorods could not occur in the absence of oleic acid.

The uniqueness of our approach lies in the ability to originally conserve the rod shape of the parent chitin nanocrystals in the nanocarbon semiconductors with photoluminescent properties. The anisotropic shape integrity achieved upon carbonization may be due to the high crystallinity of chitin nanorods. We also note that dilute solutions of chitin nanorods (*e.g.*, 0.5 wt%) can be used as a precursor aqueous phase for preparing the luminescent oleic acid-capped carbon nanorods dispersed in toluene with their lower concentrations. In this work, we

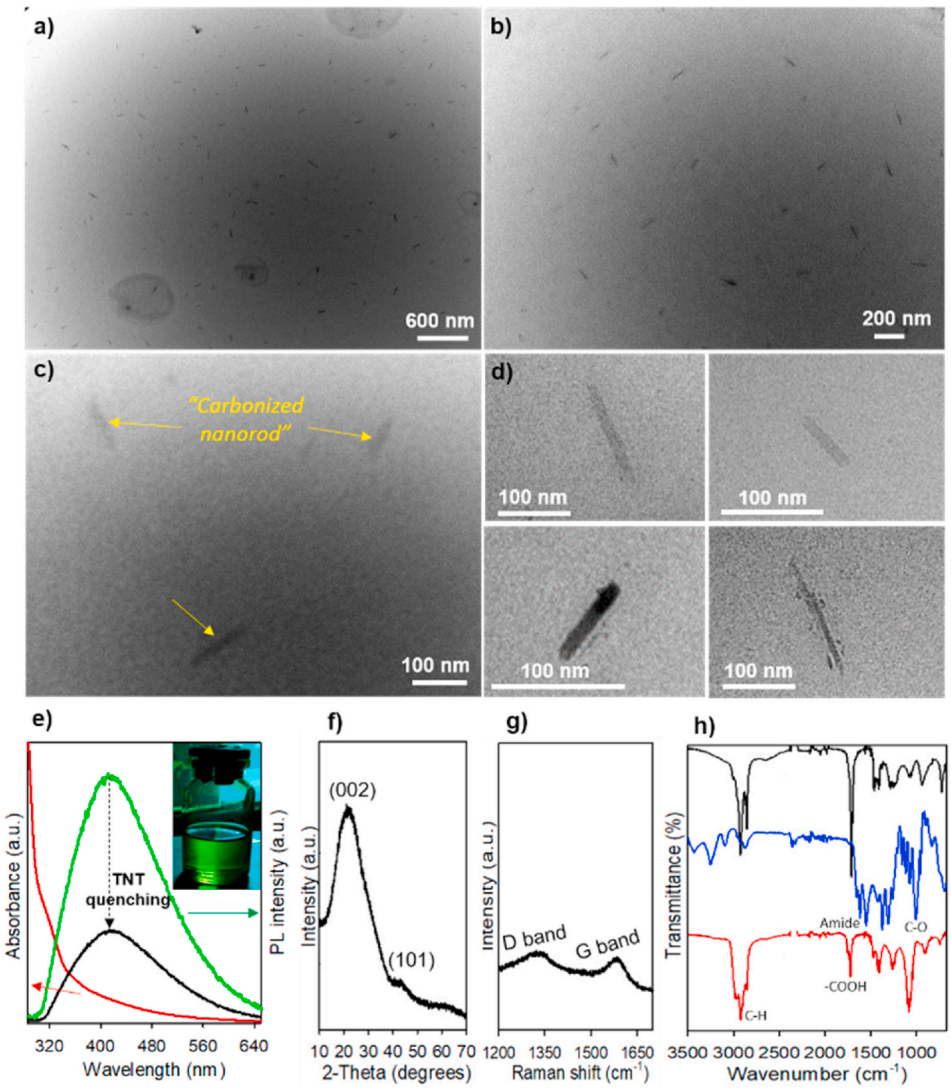

Fig. 7. Structural features of luminescent oleic acid-capped carbon nanorods prepared by hydrothermal liquid crystal transfer. (a–d) TEM images of oleic acid-capped carbon nanorods viewed at different magnifications, (e) UV–Vis spectrum and Photoluminescence spectra (excitation wavelength at 300 nm) of oleic acid-capped carbon nanorods dispersed in toluene; the photoluminescent signal is considerably quenched in the presence of 20 μM trinitrotoluene as indicated in black line, (f) PXRD pattern and (g) Raman spectrum of oleic acid-capped carbon nanorods, and (h) IR spectra of free oleic acid (black), chitin nanocrystals (blue), and oleic acid-capped carbon nanorods (red).

preferred to use directly chitin liquid crystals (higher concentration of chitin (6.6 wt%)) to obtain the higher concentration carbonized dispersion because of the increased phase transfer at higher precursor concentrations.

Although many efforts have been made to develop carbon nanoparticles from the hydrothermal carbonization of carbohydrates, most of them are prepared in water to obtain nanocarbons that mostly dispersed in water [42,67]. Until now, there is only one literature recently reported by Bhunia et al. on the hydrothermal carbonization of the usual carbohydrate sources into hydrophobic luminescent nanocarbons [68]. However, these materials are nanodots rather than anisotropic shaped nanoparticles (*e.g.,* nanorods). To the best of our knowledge, this is the first experiment of using chitin liquid crystals in the biphasic system to generate the luminescent non-polar colloidal dispersion of the new oleic

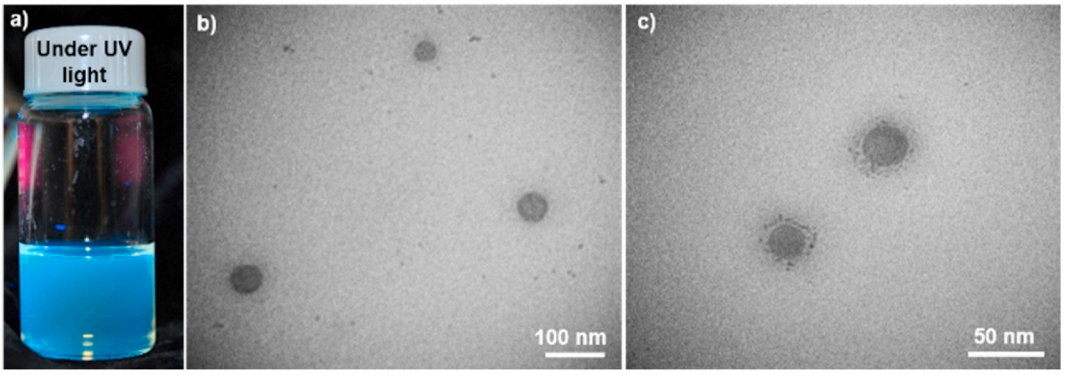

Fig. 8. Two-phase transfer synthesis of acidic chitosan solution as a water phase. (a) Photo and (b,c) TEM images of photoluminescent carbon dot-shaped nanoparticles dispersed in toluene instead of carbon rod-shaped nanoparticles.

acid-capped carbon nanorods by hydrothermal phase transfer carbonization. It surprised to realize the intense photoluminescence of the carbon rod-shaped nanoparticles, even though their particle sizes are larger than those of previously reported carbon nanodots. These features may be dominated by their surface properties and anisotropic features.

To evaluate which factors are key to the formation of the carbonized nanorods, we carried out a control experiment of using an acidic chitosan solution (~6.6 wt%) instead of chitin liquid crystals under the exact same reaction conditions. After hydrothermal treatment, the homogeneous upper phase also shows lightly green luminescence with lower intensity (Fig. 8a). However, TEM examination indicated that all solid material dispersed in toluene is carbon nanodots with an average size of ~20–40 nm (Fig. 8b and c). No nanorods could be observed in this sample. The formation of the carbon nanodots from the conventional chitosan solution in the biphasic mixture is similar to Yang et al.'s report on the hydrothermal carbonization of chitosan in an one-phase aqueous solution [61].

Chitosan often forms by hot alkali deacetylation of chitin. The release of acetyl groups typically leads to the decreased crystallinity and acidic dissolution of chitosan. These features make soft chitosan macromolecules less thermal stable and more easily to be decomposed to smaller intermediates that could convert to carbonized nanodots by hydrothermal liquid crystal transfer carbonization. Conversely, the robust rod-shaped chitin nanocrystals were formed from the selective removal of amorphous regions in natural chitin nanofibrils by acid hydrolysis. This reaction allows to obtain the highly crystalline chitin nanorods that likely do not dissolve in acidic media, but disperse in water. The additional experiment convinces that the high crystallinity and mechanical rigidity of the chitin nanorods are key to increase their thermal and chemical stability, thus being the shape integrity of the carbonized nanorods. We also performed the hydrothermal two-phase transfer of cellulose liquid crystals under the same reaction conditions, but the resultant sample obtained at the very lower concentration and showed poor photoluminescent color. These results might be due to weak interactions between cellulose nanocrystals and oleic acid and the absence of nitrogen doping in the cellulose-derived carbon nanoparticles.

It is worthy to mention that the new carbon nanorods possess the nature of the amorphous graphite, but they are non-black in color. The appearance of the light brown colors in the colloidal dispersion may be related to the nanoscale size, monodispersity, and colloidal stability of the oleic acid-capped carbon nanorods. Taking advantages of the solid-liquid phase transfer approach, these hydrophobic carbonized nanorods hold promise as targets for the design of functional materials for useful applications [69]. The hydrophobic surface may allow the carbonized nanorods functional as catalyst supports to access non-polar solvents in order to perform catalytic reactions of organic compounds in the organic synthesis chemistry [70]. The colloidal monodispersity may enable to couple the carbonized nanorods with secondary nanoparticles by surface attachment to create functionalities [71,72]. Moreover, the photoluminescent carbon nanorod dispersion could be a novel solution for optical coating in solid-state materials to exploit its optoelectronic property for sensing applications. Evidently, we designed colorful light emitting glasses from the evaporation-induced self-assembly of the oleic acid-stabilized carbon nanorod colloids on a silica substrate (Fig. 6g).

4. Conclusions

In summary, the biomimetic conversion of twisted Bouligand structure and the role of carbon in chitin nanofibrils in abundantly discarded crab shells have been inspired to make new types of sustainable optoelectronic carbon-based nanostructures. Chitin in the originally mineralized crab shell was carbonized to yield helical mesoporous carbon replica that homogeneously decorated with cobalt oxide nanoparticles to show their electrochemical supercapacitance, and could potentially extend to electrocatalysis and gas sensing as well. Beyond structural mimicry, colloidal chemistry of hydrophobic carbon nanorods with photoluminescent emission was exploited from chitin liquid crystals derived from crab shell. Oleic acid-stabilized carbonaceous nanorods can be formed by hydrothermal phase transfer of chitin liquid crystals in water into toluene in the assistance of oleic acid as a phase transferring agent and a capping agent. It surprised to find that the hydrothermal phase transfer carbonization of amphiphilic chitin nanorods structurally preserves their anisotropic shape and nanoscale size to generate hydrophobic carbon rod-shaped nanoparticles with brilliant green luminescent emission. Our inspiration shows the first experiment of anisotropic chitin LC-to-carbon conversion based on two-phase transfer system, and consequently forming a new type of hydrophobic carbon nanorod colloids with optical response. The hydrophobicity, anisotropy, monodispersity, and photoluminescence endow the sustainable chitin liquid crystal-derived carbonaceous nanomaterials with unique features of surface functionalization and layer coating for applications in photocatalysis, optical sensing, and nano-colloidal coating.

CRediT authorship contribution statement

Trang The Lieu Chau: Conceptualization, Methodology, Data curation, Writing – original draft. **Tuyen Phi Vu:** Conceptualization, Software, Writing – original draft, Funding acquisition. **Hoa Thi Le:** Formal analysis, Data curation. **Do Van Phan:** Investigation, Software. **Ca Xuan Nguyen:** Formal analysis, Software. **Thanh Duy Luong:** Investigation, Software. **Phuong Thi Anh Le:** Investigation, Software. **Nhan Thi Thanh Dang:** Formal analysis, Software. **Long Viet Nguyen:** Formal analysis, Software. **Nguyen Duc Cuong:** Conceptualization, Methodology, Supervision, Writing – original draft, Writing – review & editing.

Declaration of competing interest

The authors declare that they have no known competing financial interests or personal relationships that could have appeared to influence the work reported in this paper.

Acknowledgements

This research is funded by Vietnam National Foundation for Science and Technology Development (NAFOSTED) under grant number 103.02-2018.365.

Appendix A. Supplementary data

Supplementary data to this article can be found online at https://doi.org/10.1016/j.optmat.2021.111100.

References

[1] C.R. Kagan, L.E. Fernandez, Y. Gogotsi, P.T. Hammond, M.C. Hersam, A.E. Nel, R. M. Penner, C.G. Willson, P.S. Weiss, Nano day: celebrating the next decade of nanoscience and nanotechnology, ACS Nano 10 (2016) 9093–9103.
[2] M. Yoshida, J. Lahann, Smart nanomaterials, ACS Nano 2 (2008) 1101–1107.
[3] N.D. Cuong, D.T. Quang, Progress through synergistic effects of heterojunction in nanocatalysts - review, Vietnam J. Chem. 58 (2020) 434–463.
[4] W.-T. Koo, J.E. Millstone, P.S. Weiss, I.-D. Kim, The design and science of polyelemental nanoparticles, ACS Nano 14 (2020) 6407–6413.
[5] O. Kozák, M. Sudolská, G. Pramanik, P. Cígler, M. Otyepka, R. Zbořil, Photoluminescent carbon nanostructures, Chem. Mater. 28 (2016) 4085–4128.
[6] T.D. Nguyen, From formation mechanisms to synthetic methods toward shape-controlled oxide nanoparticles, Nanoscale 5 (2013) 9455–9482.
[7] D. Sun, C. Liu, W. Ren, H. Cheng, All-carbon thin-film transistors as a step towards flexible and transparent electronics, Adv. Electron. Mater. 2 (2016), 1600229.
[8] Y. Wang, A. Hu, Carbon quantum dots: synthesis, properties and applications, J. Mater. Chem. C. 2 (2014) 6921.
[9] M.S. Mauter, M. Elimelech, Environmental applications of carbon-based nanomaterials, Environ. Sci. Technol. 42 (2008) 5843–5859.
[10] A.J. Clancy, M.K. Bayazit, S.A. Hodge, N.T. Skipper, C.A. Howard, M.S.P. Shaffer, Charged carbon nanomaterials: redox chemistries of fullerenes, carbon nanotubes, and graphenes, Chem. Rev. 118 (2018) 7363–7408.

[11] L. Cheng, C. Wang, L. Feng, K. Yang, Z. Liu, Functional nanomaterials for phototherapies of cancer, Chem. Rev. 114 (2014) 10869–10939.
[12] D.S. Su, S. Perathoner, G. Centi, Nanocarbons for the development of advanced catalysts, Chem. Rev. 113 (2013) 5782–5816.
[13] T. Umeyama, H. Imahori, Photofunctional hybrid nanocarbon materials, J. Phys. Chem. C 117 (2013) 3195–3209.
[14] W. Yang, S. Chen, Biomass-derived carbon for electrode fabrication in microbial fuel cells: a review, Ind. Eng. Chem. Res. 59 (2020) 6391–6404.
[15] R.S. Varma, Biomass-derived renewable carbonaceous materials for sustainable chemical and environmental applications, ACS Sustain. Chem. Eng. 7 (2019) 6458–6470.
[16] M.-M. Titirici, R.J. White, N. Brun, V.L. Budarin, D.S. Su, F. del Monte, J.H. Clark, M.J. MacLachlan, Sustainable carbon materials, Chem. Soc. Rev. 44 (2015) 250–290.
[17] B. Kang, T. Opatz, K. Landfester, F.R. Wurm, Carbohydrate nanocarriers in biomedical applications: functionalization and construction, Chem. Soc. Rev. 44 (2015) 8301–8325.
[18] H. Yang, N. Yan, Transformation of seafood wastes into chemicals and materials, in: Encycl. Sustain. Sci. Technol., Springer, New York, New York, NY, 2018, pp. 1–23.
[19] N. Suryawanshi, S.E. Jujjavarapu, S. Ayothiraman, Marine shell industrial wastes–an abundant source of chitin and its derivatives: constituents, pretreatment, fermentation, and pleiotropic applications-a revisit, Int. J. Environ. Sci. Technol. 16 (2019) 3877–3898.
[20] T. Hahn, E. Tafi, A. Paul, R. Salvia, P. Falabella, S. Zibek, Current state of chitin purification and chitosan production from insects, J. Chem. Technol. Biotechnol. 95 (2020) 2775–2795.
[21] J.L. Shamshina, P. Berton, R.D. Rogers, Advances in functional chitin materials: a review, ACS Sustain. Chem. Eng. 7 (2019) 6444–6457.
[22] X. Zhang, M. Rolandi, Engineering strategies for chitin nanofibers, J. Mater. Chem. B. 5 (2017) 2547–2559.
[23] Y. Bouligand, Twisted fibrous arrangements in biological materials and cholesteric mesophases, Tissue Cell 4 (1972) 189–217.
[24] M. Nogi, F. Kurosaki, H. Yano, M. Takano, Preparation of nanofibrillar carbon from chitin nanofibers, Carbohydr. Polym. 81 (2010) 919–924.
[25] J. Zhou, L. Bao, S. Wu, W. Yang, H. Wang, Chitin based heteroatom-doped porous carbon as electrode materials for supercapacitors, Carbohydr. Polym. 173 (2017) 321–329.
[26] H.S. Kim, M.S. Kang, W.C. Yoo, Co3O4 nanocrystals on crab shell-derived carbon nanofibers (Co3O4 @CSCNs) for high-performance supercapacitors, Bull. Kor. Chem. Soc. 39 (2018) 327–334.
[27] S.Y. Son, S.-A. Hong, S.Y. Oh, Y.-C. Lee, G.-W. Lee, J.W. Kang, Y.S. Huh, I.T. Kim, Crab-shell biotemplated SnO2 composite anodes for lithium-ion batteries, J. Nanosci. Nanotechnol. 18 (2018) 6463–6468.
[28] S. Zheng, J. Zhang, H. Deng, Y. Du, X. Shi, Chitin derived nitrogen-doped porous carbons with ultrahigh specific surface area and tailored hierarchical porosity for high performance supercapacitors, J. Bioresour. Bioprod. (2021), https://doi.org/10.1016/j.jobab.2021.02.002 (in press).
[29] G.A. Jeffrey, Carbohydrate liquid crystals, Acc. Chem. Res. 19 (1986) 168–173.
[30] V. Vill, R. Hashim, Carbohydrate liquid crystals: structure–property relationship of thermotropic and lyotropic glycolipids, Curr. Opin. Colloid Interface Sci. 7 (2002) 395–409.
[31] J.-F. Revol, R.H. Marchessault, In vitro chiral nematic ordering of chitin crystallites, Int. J. Biol. Macromol. 15 (1993) 329–335.
[32] V.S. Yeul, S.S. Rayalu, Unprecedented chitin and chitosan: a chemical overview, J. Polym. Environ. 21 (2013) 606–614.
[33] T.T.L. Chau, D.Q.T. Le, H.T. Le, C.D. Nguyen, L.V. Nguyen, T.D. Nguyen, Chitin liquid-crystal-templated oxide semiconductor aerogels, ACS Appl. Mater. Interfaces 9 (2017) 30812–30820.
[34] L. Gao, L. Xiong, D. Xu, J. Cai, L. Huang, J. Zhou, L. Zhang, Distinctive construction of chitin-derived hierarchically porous carbon microspheres/polyaniline for high-rate supercapacitors, ACS Appl. Mater. Interfaces 10 (2018) 28918–28927.
[35] L. Gao, G. Zhang, J. Cai, L. Huang, J. Zhou, L. Zhang, Rationally exfoliating chitin into 2D hierarchical porous carbon nanosheets for high-rate energy storage, Nano Res. 13 (2020) 1604–1613.
[36] F. Gao, J. Qu, C. Geng, G. Shao, M. Wu, Self-templating synthesis of nitrogen-decorated hierarchical porous carbon from shrimp shell for supercapacitors, J. Mater. Chem. A. 4 (2016) 7445–7452.
[37] X. Wang, Y. Feng, P. Dong, J. Huang, A mini review on carbon quantum dots: preparation, properties, and electrocatalytic application, Front. Chem. 7 (2019).
[38] W. Meng, X. Bai, B. Wang, Z. Liu, S. Lu, B. Yang, Biomass-derived carbon dots and their applications, Energy Environ. Mater. 2 (2019) 172–192.
[39] C. Falco, F. Perez Caballero, F. Babonneau, C. Gervais, G. Laurent, M.-M. Titirici, N. Baccile, Hydrothermal carbon from biomass: structural differences between hydrothermal and pyrolyzed carbons via 13 C solid state NMR, Langmuir 27 (2011) 14460–14471.
[40] Y. Huang, S. Hu, S. Zuo, Z. Xu, C. Han, J. Shen, Mesoporous carbon materials prepared from carbohydrates with a metal chloride template, J. Mater. Chem. 19 (2009) 7759.
[41] N. Shi, Q. Liu, X. He, G. Wang, N. Chen, J. Peng, L. Ma, Molecular structure and formation mechanism of hydrochar from hydrothermal carbonization of carbohydrates, Energy Fuels 33 (2019) 9904–9915.
[42] B. Hu, K. Wang, L. Wu, S.-H. Yu, M. Antonietti, M.-M. Titirici, Engineering carbon materials from the hydrothermal carbonization process of biomass, Adv. Mater. 22 (2010) 813–828.
[43] Z. Zhang, W. Sun, P. Wu, Highly photoluminescent carbon dots derived from egg white: facile and green synthesis, photoluminescence properties, and multiple applications, ACS Sustain. Chem. Eng. 3 (2015) 1412–1418.
[44] N.T.T. Dang, T.T.L. Chau, H. Van Duong, H.T. Le, T.T. Van Tran, T.Q. Le, T.P. Vu, C.D. Nguyen, L.V. Nguyen, T.-D. Nguyen, Water-soluble chitosan-derived sustainable materials: towards filaments, aerogels, microspheres, and plastics, Soft Matter 13 (2017) 7292–7299.
[45] A.M. Molodets, A.A. Golyshev, Structural transformations of amorphous carbon (glassy carbon) at high shock pressures, J. Exp. Theor. Phys. 126 (2018) 772–778.
[46] W. Gao, Y. Wan, Y. Dou, D. Zhao, Synthesis of partially graphitic ordered mesoporous carbons with high surface areas, Adv. Energy Mater. 1 (2011) 115–123.
[47] Q. Wang, D.D. Allred, L.V. Knight, Deconvolution of the Raman spectrum of amorphous carbon, J. Raman Spectrosc. 26 (1995) 1039–1043.
[48] X. Zhu, H. Ji, J. Yi, J. Yang, X. She, P. Ding, L. Li, J. Deng, J. Qian, H. Xu, H. Li, A specifically exposed cobalt oxide/carbon nitride 2D heterostructure for carbon dioxide photoreduction, Ind. Eng. Chem. Res. 57 (2018) 17394–17400.
[49] J. Sun, Y. Yang, J. Wang, Z. Zhang, J. Guo, In-situ construction of cobalt oxide/nitrogen-doped porous carbon compounds as efficient bifunctional catalysts for oxygen electrode reactions, J. Alloys Compd. 827 (2020), 154308.
[50] C. Du, Y. Gao, J. Wang, W. Chen, A new strategy for engineering a hierarchical porous carbon-anchored Fe single-atom electrocatalyst and the insights into its bifunctional catalysis for flexible rechargeable Zn–air batteries, J. Mater. Chem. A. 8 (2020) 9981–9990.
[51] J. Mei, T. Liao, G.A. Ayoko, J. Bell, Z. Sun, Cobalt oxide-based nanoarchitectures for electrochemical energy applications, Prog. Mater. Sci. 103 (2019) 596–677.
[52] N. Iqbal, X. Wang, J. Ge, J. Yu, H.-Y. Kim, S.S. Al-Deyab, M. El-Newehy, B. Ding, Cobalt oxide nanoparticles embedded in flexible carbon nanofibers: attractive material for supercapacitor electrodes and CO 2 adsorption, RSC Adv. 6 (2016) 52171–52179.
[53] R. Madhu, V. Veeramani, S.-M. Chen, A. Manikandan, A.-Y. Lo, Y.-L. Chueh, Honeycomb-like porous carbon–cobalt oxide nanocomposite for high-performance enzymeless glucose sensor and supercapacitor applications, ACS Appl. Mater. Interfaces 7 (2015) 15812–15820.
[54] N. Zhao, W. Nie, X. Liu, S. Tian, Y. Zhang, X. Ji, Shape- and size-controlled synthesis and dependent magnetic properties of nearly monodisperse Mn3O4 nanocrystals, Small 4 (2008) 77–81.
[55] S. Mandal, M. Rakibuddin, R. Ananthakrishnan, Strategic synthesis of SiO 2 -modified porous Co 3 O 4 nano-octahedra through the nanocoordination polymer route for enhanced and selective sensing of H 2 gas over NO x, ACS Omega 3 (2018) 648–661.
[56] Z. Guo, J. Wang, F. Qin, L. Ge, Z. Li, W. Shen, Controlled chiral transcription and efficient separation via graphene oxide encapsulated helical supramolecular assembly, ACS Sustain. Chem. Eng. 8 (2020) 3401–3411.
[57] Y. Zhang, M. Qin, C. Zhao, X. Dou, C. Xing, M. Sun, X. Ma, C. Feng, Controlled chiral transcription and efficient separation via graphene oxide encapsulated helical supramolecular assembly, Carbon N. Y. 165 (2020) 82–89.
[58] M. Perovic, S.S. Aloni, Y. Mastai, M. Oschatz, Mesoporous carbon materials with enantioselective surface obtained by nanocasting for selective adsorption of chiral molecules from solution and the gas phase, Carbon N. Y. 170 (2020) 550–557.
[59] H. Wang, Y. Yuan, L. Wei, K. Goh, D. Yu, Y. Chen, Catalysts for chirality selective synthesis of single-walled carbon nanotubes, Carbon N. Y. 81 (2015) 1–19.
[60] B. Alonso, E. Belamie, Chitin-silica nanocomposites by self-assembly, Angew. Chem. Int. Ed. 49 (2010) 8201–8204.
[61] Y. Yang, J. Cui, M. Zheng, C. Hu, S. Tan, Y. Xiao, Q. Yang, Y. Liu, One-step synthesis of amino-functionalized fluorescent carbon nanoparticles by hydrothermal carbonization of chitosan, Chem. Commun. 48 (2012) 380–382.
[62] Q. Jiang, Y. Jing, Y. Ni, R. Gao, P. Zhou, Potentiality of carbon quantum dots derived from chitin as a fluorescent sensor for detection of ClO−, Microchem. J. 157 (2020), 105111.
[63] T.-D. Nguyen, B.U. Peres, R.M. Carvalho, M.J. MacLachlan, Photonic hydrogels from chiral nematic mesoporous chitosan nanofibril assemblies, Adv. Funct. Mater. 26 (2016) 2875–2881.
[64] T.-D. Nguyen, T.-O. Do, General two-phase routes to synthesize colloidal metal oxide nanocrystals: simple synthesis and ordered self-assembly structures, J. Phys. Chem. C 113 (2009) 11204–11214.
[65] T.-D. Nguyen, D. Mrabet, T.-O. Do, Controlled self-assembly of Sm 2 O 3 nanoparticles into nanorods: simple and large scale synthesis using bulk Sm 2 O 3 powders, J. Phys. Chem. C 112 (2008) 15226–15235.
[66] T.-D. Nguyen, K.E. Shopsowitz, M.J. MacLachlan, Mesoporous nitrogen-doped carbon from nanocrystalline chitin assemblies, J. Mater. Chem. A. 2 (2014) 5915.
[67] L. Yu, C. Falco, J. Weber, R.J. White, J.Y. Howe, M.-M. Titirici, Carbohydrate-derived hydrothermal carbons: a thorough characterization study, Langmuir 28 (2012) 12373–12383.
[68] S.K. Bhunia, A. Saha, A.R. Maity, S.C. Ray, N.R. Jana, Carbon nanoparticle-based fluorescent bioimaging probes, Sci. Rep. 3 (2013) 1473.
[69] K.M. Noone, D.S. Ginger, Doping for speed: colloidal nanoparticles for thin-film optoelectronics, ACS Nano 3 (2009) 261–265.

[70] A. Bahuguna, A. Kumar, V. Krishnan, Carbon-support-based heterogeneous nanocatalysts: synthesis and applications in organic reactions, Asian J. Org. Chem. 8 (2019) 1263–1305.
[71] C.J. Murphy, A.M. Vartanian, F.M. Geiger, R.J. Hamers, J. Pedersen, Q. Cui, C. L. Haynes, E.E. Carlson, R. Hernandez, R.D. Klaper, G. Orr, Z. Rosenzweig, Biological responses to engineered nanomaterials: needs for the next decade, ACS Cent. Sci. 1 (2015) 117–123.
[72] M. Grzelczak, J. Vermant, E.M. Furst, L.M. Liz-Marzán, Directed self-assembly of nanoparticles, ACS Nano 4 (2010) 3591–3605.